Habitable-zone exoplanet observatory (HabEx) baseline 4-m telescope design and predicted performance

H. Philip Stahl,[a] Gary Kuan[b],

Willian Arnold,[c] Mike Baysinger,[d] Thomas Brooks,[a] Velibor Cormarkovic,[b] Jacqueline Davis,[a] Jay Garcia,[d] Jonathan Gaskin,[e] J. Brent Knight,[a] Stefan Martin,[b] Jonathan McCready,[f] Navtej Saini,[b] Hao Tang,[g] and Juan Villalvazo,[b].

[a] NASA MARSHALL SPACE FLIGTH CENTER, HUNTSVILLE, AL 35812
[b] JET PROPULSION LABORATORY, PASADINA, CA 91109
[c] AI SOLUTIONS, HUNTSVILLE, AL 35812;
[d] ESSA, HUNTSVILLE, AL 35812;
[e] UNIVERSITY OF NORTH CAROLINE CHARLOTTE;
[f] NORTH CAROLINA STATE UNIVERSITY; AND [g] UNIVERSITY OF MICHIGAN

ABSTRACT

The Habitable Exoplanet Observatory Mission (HabEx) is one of four missions under study for the 2020 Astrophysics Decadal Survey. Its goal is to directly image and spectroscopically characterize planetary systems in the habitable zone around nearby sun-like stars. Additionally, HabEx will perform a broad range of general astrophysics science enabled by 100 to 2500 nm spectral range and 3 x 3 arc-minute FOV. Critical to achieving its the HabEx science goals is a large, ultra-stable UV/Optical/Near-IR (UVOIR) telescope. The baseline HabEx telescope is a 4-meter off-axis unobscured three-mirror-anastigmatic, diffraction limited at 400 nm with wavefront stability on the order of a few 10s of picometers. This paper summarizes the opto-mechanical design of the HabEx baseline optical telescope assembly, including a discussion of how science requirements drive the telescope's specifications, and presents analysis that the baseline telescope structure meets its specified tolerances.

Keywords: space telescopes, astrophysics, astronomy, HabEx

1. INTRODUCTION

"Are we alone in the Universe?" maybe the most compelling science question of our generation. Per the 2010 *New Worlds, New Horizons* Decadal Report[1]: "One of the fastest growing and most exciting fields in astrophysics is the study of planets beyond our solar system. The ultimate goal is to image rocky planets that lie in the habitable zone of nearby stars." The Survey recommended, as its highest priority, medium-scale activity such as a "New Worlds Technology Development Program" to "lay the technical and scientific foundations for a future space imaging and spectroscopy mission." As a result, NASA is studying in detail the Habitable Exoplanet Observatory Mission (HabEx) for the 2020 Decadal Survey. HabEx has three goals: to seek out nearby worlds and explore their habitability; to map out nearby planetary systems and understand the diversity of the worlds they contain; and, to carry out observations that open up new windows on the universe from the UV through near-IR. The HabEx Science and Technology Definition Team has selected a baseline architecture of a 4-meter telescope with four science instruments (coronagraph, star-shade instrument, UV-NIR imaging multi-object slit spectrograph, and high resolution UV spectrograph) and a 72-m external star-shade occulter.

Telescope design is an iterative process. In 2017, we published a paper that provided an overview of an initial HabEx telescope design concept, our design process and a performance evaluation for the concept.[2] And, in 2018, we published a paper describing the features and performance predictions for a significantly modified Baseline Rev 1 design.[3] This paper describes the features and predicted performance (line of sight, mechanical and thermal wavefront stability) for the final Baseline 4-m telescope design. Section 2 reviews how the HabEx OTA specifications are derived from the HabEx science requirements. Section 3 describes the baseline opto-mechanical OTA design, its key components and design features. Finally, Section 4 summarizes detailed performance analysis of the baseline opto-mechanical design which shows that the design, using proven technology and engineering practice, can achieve the specifications necessary to perform HabEx science. The baseline 4-m off-axis HabEx opto-mechanical telescope design 'closes' for its line-of-sight (LOS) and wavefront error (WFE) stability specifications. The only external assumptions is that the mission is launched in an SLS 8.4-m fairing and uses low disturbance micro-thrusters for pointing control.

2. OPTICAL TELESCOPE ASSEMBLY SPECIFICATIONS

The optical telescope design form and its performance specifications (Table 1) are derived from science requirements.

Table 1: HabEx Optical Telescope Specification	
Specification	Value
Architecture	Off-Axis Unobscured Circular Aperture
Optical Design	Three-Mirror Anastigmatic
Science Instruments	On the side, in the Secondary Mirror Tower structure
Aperture Diameter	> 4.0 meters
Primary Mirror F/#	F/2.5 or slower
Diffraction Limited Wavelength	400 nm
Line of Sight Stability (Jitter)	< 0.5 milli-arc-seconds per axis
Wavefront Error Stability	1 to 250 pm depending on coronagraph and spatial frequency

Exoplanet science drives the choice of an off-axis architecture, aperture diameter and primary mirror F/#. General astrophysics' desire for a 3 x 3 arcminute field of view (FOV) drives the choice of a three mirror anastigmatic (TMA) optical design and spectral range. Both exoplanet and general astrophysics science need 400 nm diffraction limited. LOS Jitter and WFE stability are discussed in Sections 2.1 and 2.2.

Imaging habitable zone exoplanets using a coronagraph requires a telescope/coronagraph system that produces a 10^{-10} dark-hole with as small of an inner working angle (IWA) as possible and as large of an irradiance throughput as possible. The smaller the IWA and the larger the throughput, the greater the number of habitable zones that can be searched. The ability to achieve a small IWA depends upon the telescope's ability to produce a small stable point spread function (PSF) with a compact stable encircled energy (EE). The smaller the EE, the smaller the IWA. It is common knowledge that the larger a telescope's aperture, the smaller its PSF and EE. But, what is often overlooked is that an unobscured (off-axis) telescope always has a more compact EE (better IWA) than an on-axis telescope with a central obscuration – because diffraction from the central obscuration broadens the PSF. To be specific, an unobscured circular aperture has 82.8% EE at λ/D. And, a telescope with a 10% central obscuration has 82.5% EE at 1.4 λ/D (and for a 20% obscuration, 82% EE is at 1.63 λ/D).[4] Thus to achieve the same IWA as an unobscured 4-m telescope, an on-axis telescope with 10% central obscuration needs to be at least 5.6-m and one with 20% obscuration needs to be at least 6.5-m. Additionally, diffraction from secondary mirror spider obscurations distort the PSF and broaden the EE. A 1 to 2% wide spider can increase EE diameter (IWA) by 5 to 10%[4] – requiring a 5 to 10% larger on-axis telescope. Of course the problem is even worse for a segmented aperture primary mirror. Figure 1 shows the core throughput for three different coronagraphs: vector-vortex charge 4 (VVC4), vector-vortex charge 6 (VVC6) and hybrid Lyot (HLC) with the HabEx baseline 4-meter off-axis unobscured telescope; and, the throughput for a 6-m on-axis segmented primary mirror telescope (i.e. JWST) with an apodized pupil Lyot coronagraph (APLC).[5]

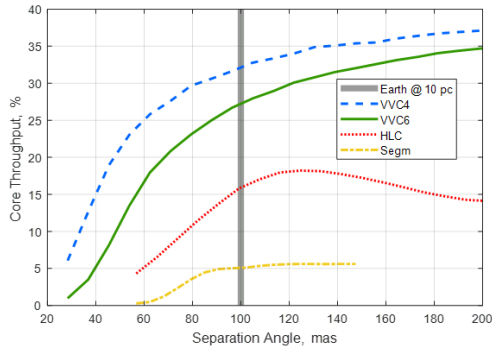

Figure 1: Core throughput versus separation angle. Vertical line is Exo-Earth at 10 pc (100 mas).[5]

Regarding minimum aperture and diffraction limit, the specification is based on a design reference mission yield estimate for an off-axis-telescope/coronagraph combination.[6] Threshold science occurs when the telescope PSF core radius (λ/D) is 20 mas. This is accomplished with a 4-m off-axis monolithic telescope with a 400 nm diffraction limit. And, while a larger aperture would provide higher yield, 4-m was selected as the baseline for programmatic reasons. First, 4-m mirrors are manufacturable. Schott has infrastructure to melt and cast 4.2-m diameter by 42 cm thick Zerodur® mirror substrates. And, Corning has infrastructure to either frit bond or low-temperature-fuse 4-m 'class' ULE® mirror substrates. And, at least four organizations have existing infrastructure to grind and polish 4-m class substrates into space mirrors, including: Collins Aerospace in Danbury CT, L3/Brashears in Pittsburgh, University of Arizona in Tucson and RESOC outside of Paris France. Second, a 4-m class telescope can be packaged inside of NASA's planned SLS 8.4-m fairing.

Regarding the primary mirror's F/#, to minimize package size, a fast PM F/# or short radius of curvature is desired. But, to minimize polarization cross-talk in the coronagraph, a slow PM F/# is required. After consideration, an optical design similar to Exo-C with an F/2.5 primary mirror and the science instruments located on the anti-Sun side of the telescope[7]

was selected. This configuration minimizes the need for high incidence angle reflections that produce unwanted polarization effects and isolates the coronagraph from thermal disturbances. As a consequence, the OTA is physically long. The baseline 4-m design has a primary to secondary mirror separation of ~9-m.

2.1 Line of Sight (LOS) Stability Specification

LOS instability is important for both general astrophysics and coronagraphy because it causes PSF smearing that degrades spatial resolution and IWA. A typical specification for LOS error is less than 1/10th the point spread function (PSF) radius. For a 400 nm diffraction limited 4-m telescope, the on-sky PSF radius is 25 mas. Thus, the specification should be < 2.5 mas. But, coronagraphs require LOS stability better than 0.5 mas per axis. The reason is that LOS error causes beam-shear on the secondary and tertiary mirrors, as well as other mirrors in the optical train, which introduces WFE that result in contrast leakage (see Section 2.2).

Sources of LOS instability are thermal and mechanical. LOS drift occurs when the telescope slews relative to the Sun. Temperature change causes the telescope structure to expand or contract resulting in rigid-body motions of the optical components relative to each other. Fortunately, thermal effects are slow and can be corrected. HabEx is baselining a laser-truss system to sense and correct LOS drift. LOS jitter is more important. Jitter is produced when mechanical disturbance accelerations excite modes in the telescope structure causing rigid body motions of the primary and secondary mirrors. HabEx is baselining a low-order wavefront-sensor (LOWFS) that can sense and correct LOS jitter on the order of 2.5 mas to < 0.5 mas per axis at frequencies below 10 Hz.[9] But, given that the LOWFS cannot correct jitter at frequencies above 10-Hz, the LOS stability must be stable to < 0.5 mas for frequencies above 10-Hz.

Specification				56.00	mas
				ALLOCATION (one sided PV)	
Alignment	ZEMAX	Tolerance	units	RSS	Units
PM X-Decenter	DX	10	nanometer	17.20	mas
PM Y-Decenter	DY	10	nanometer	16.70	mas
PM Z-Despace	DZ	10	nanometer	4.30	mas
PM Y-Tilt	TX	0.5	nano-radian	17.32	mas
PM X-Tilt	TY	0.5	nano-radian	17.05	mas
PM Z-Rotation	TZ	0.5	nano-radian	2.15	mas
SM X-Decenter	DX	20	nanometer	30.60	mas
SM Y-Decenter	DY	20	nanometer	29.60	mas
SM Z-Despace	DZ	20	nanometer	8.60	mas
SM Y-Tilt	TX	1	nano-radian	3.05	mas
SM X-Tilt	TY	1	nano-radian	3.00	mas
SM Z-Rotation	TZ	1	nano-radian	0.33	mas
TM X-Decenter	DX	10	nanometer	1.90	mas
TM Y-Decenter	DY	10	nanometer	1.90	mas
TM Z-Despace	DZ	1000	nanometer	0.00	mas
TM Y-Tilt	TX	10	nano-radian	4.17	mas
TM X-Tilt	TY	10	nano-radian	4.17	mas
TM Z-Rotation	TZ	1000	nano-radian	0.74	mas
RSS LOS Error				56.00	mas

Figure 2: Rigid body motion allocation to meet < 0.7 mas on-sky LOS Stability specification.

To design the telescope, it is necessary to convert the LOS stability specification into an engineering specification, i.e. maximum allowed mirror rigid body motions. Zemax tolerance analysis provides the LOS and WFE sensitivity to rigid body motions of the primary, secondary and tertiary mirror for the baseline F/2.5 optical design.[2,3] From these sensitivities, an LOS error budget can be allocated for each rigid body degree of freedom (DOF) to keep the on-sky LOS jitter blur circle < 0.7 mas. Figure 2 shows one potential error budget allocation. Please note that Zemax tolerances are calculated at the fine-steering mirror, where, because the optical design has an 80X magnification, the LOS Stability specification is < 56 mas.

2.2 Wavefront Error (WFE) Stability Specification

WFE stability specification is driven by the coronagraph. Any temporal or dynamic change in WFE can result in dark-hole speckles that produce a false exoplanet measurement or mask a true signal. The issue is how large of a WFE can a coronagraph tolerate. A leading candidate is the Vector Vortex Coronagraph (VVC-N) where N indicates the 'charge' or azimuthal shear. The higher the 'charge' the more low order error it can tolerate, but the larger its IWA and the lower its throughput. Currently, HabEx is baselining the VVC-6. Figure 3 summarizes the maximum amount of each Zernike polynomial that can be tolerated by VVC-4 to VVC-10.[9] However, this is the maximum amount for each term 'if' that term were the only error source. In practice, it is necessary to distribute the error between all of the terms. One approach for creating an error budget is the Noise Equivalent Contrast Ratio (NECR) method.[5] Figure 4, shows a simple implementation of this method where 1-ppt of contrast ratio is allocated each to tilt, power, astigmatism, coma and spherical. And, the balance is divide between the higher order terms. When the contrast is allocated across all terms, the allocated error per term is lower than that shown in Figure 3. The final step is to sub-allocate each error tolerance between potential error sources. Again, Figure 4 shows a simple equal 33% sub-allocation between LOS, inertial and thermal sources. LOS instability occurs when LOS drift/jitter causes beam-shear on the secondary and tertiary mirrors. Because the mirrors are

Aberration	Indices		Allowable RMS wavefront error (nm) per mode			
	n	*m*	charge 4	charge 6	charge 8	charge 10
Tip-tilt	1	±1	1.1	5.9	14	26
Defocus	2	0	0.8	4.6	12	26
Astigmatism	2	±2	0.0067	1.1	0.90	5
Coma	3	±1	0.0062	0.66	0.82	5
Spherical	4	0	0.0048	0.51	0.73	6
Trefoil	3	±3	0.0072	0.0063	0.57	0.67
2nd Astig.	4	±2	0.0080	0.0068	0.67	0.73
2nd Coma	5	±1	0.0036	0.0048	0.69	0.85
2nd Spher.	6	0	0.0025	0.0027	0.84	1
Quadrafoil	4	±4	0.0078	0.0080	0.0061	0.53
2nd Trefoil	5	±3	0.0051	0.0056	0.0043	0.72
3rd Astig.	6	±2	0.0023	0.0035	0.0034	0.81
3rd Coma	7	±1	0.0018	0.0022	0.0036	1.18
3rd Spher.	8	0	0.0018	0.0018	0.0033	1.49

Garreth Ruane, June 2017

not rejected
first-order rejection
> first-order rejection

Figure 3: Wavefront Stability Required by VVC

conics, beam shear manifests itself as low-order astigmatism and coma (shear of spherical aberration is coma and sub-aperture coma appears to be astigmatism). Inertial instability occurs when the primary mirror is accelerated by mechanical disturbances causing it to react (i.e. bend) against its mounts. Consistent with intuition, the shape of this error is similar to the mirror's static (X,Y,Z) gravity sag (i.e. mirror bending when exposed to a 1G acceleration in the X,Y,Z directions). Thermal WFE instability occurs when the primary mirror's bulk temperature or temperature gradient changes. If the mirror's coefficient of thermal expansion (CTE) is completely homogeneous and constant, then a bulk temperature should only result is a defocus error. But any inhomogeneity in the mirror's CTE will result in a temperature dependent WFE.

		Allocation	100%	33%	33%	33%
Index			VVC-6 Tolerance	LOS	Inertial	Thermal
N	M	Aberration	[pm rms]	[pm rms]	[pm rms]	[pm rms]
		TOTAL RMS	4381.1	2528	2528	2528
1	1	Tilt	2342.6	1351.83	1351.83	1351.83
2	0	Power (Defocus)	1751.9	1010.98	1010.98	1010.98
2	2	Astigmatism	2121.2	1224.08	1224.08	1224.08
3	1	Coma	1888.2	1089.60	1089.60	1089.60
4	0	Spherical	1603.7	925.42	925.42	925.42
3	3	Trefoil	0.9	0.51	0.51	0.51
4	2	Sec Astigmatism	0.5	0.28	0.28	0.28
5	1	Sec Coma	0.4	0.25	0.25	0.25
6	0	Sec Spherical	0.3	0.19	0.19	0.19
4	4	Tetrafoil	0.8	0.49	0.49	0.49
5	3	Sec Trefoil	0.4	0.23	0.23	0.23
6	2	Ter Astigmatism	0.2	0.14	0.14	0.14
7	1	Ter Coma	0.2	0.12	0.12	0.12
5	5	Pentafoil	0.3	0.17	0.17	0.17
6	4	Sec Tetrafoil	0.3	0.17	0.17	0.17
7	3	Ter Trefoil	0.2	0.13	0.13	0.13
6	6	Hexafoil	0.2	0.12	0.12	0.12
7	5	Sec Pentafoil	0.2	0.12	0.12	0.12
7	7	Septafoil	0.2	0.14	0.14	0.14

Figure 4: Allocation of WFE Stability between LOS, Inertial and Thermal Sources.

3. TELESCOPE OPTO-MECHANICAL DESIGN

To meet the specified Wavefront (WFE) Stability and Line of Sight (LOS) Stability requires an ultra-stable opto-mechanical telescope. The baseline telescope architecture achieves this level of performance because of the mass and volume capacities of the planned Space Launch System (SLS). SLS mass capacity enables the design of an extremely stiff opto-mechanical structure that can align the primary, secondary and tertiary mirrors to each other and maintain that alignment. And, SLS volume capacity enables the use of a monolithic aperture off-axis primary mirror with no deployments. The current design is a result of multiple iterations over a three year period involving numerous trade studies on structure, primary mirror design, primary mirror mounting, where to locate the science instruments, etc..[10,2,3] These trades were accomplished using STOP analysis (Structural Thermal Optical Performance) to evaluate each iteration's ability to achieve the required performance specifications (LOS and WFE stability). A fundamental rule for the design was that every proposed system, subsystem or component should be at TRL-6 or higher except for the primary mirror assembly and science instruments. The result is extremely robust.

3.1 Baseline HabEx Optical Telescope

The 'baseline' telescope (Figure 5) consists of the primary mirror assembly, secondary mirror assembly, secondary mirror tower with integrated science instrument module, and stray-light tube with forward scarf. The scarf angle (currently set at 45 degrees) determine the closest angle of observation to the sun. The tower and baffle tube are the optical bench which maintains alignment between the PMA, SMA and TMA. The OTA is physically separate from the spacecraft which includes the solar array sunshield. The size of the solar arrays on the bottom are driven by thermal power requirements during anti-sun pointing. Instead of reaction wheels, thrusters are used for slewing the observatory and micro-thrusters are used for fine pointing control during science observations. The OTA and spacecraft connect only at the interface ring. This ring is also the interface between the payload and the Space Launch System (SLS). Not shown is the forward door. It is closed for launch to prevent contamination and provide additional stiffness. Additionally, launch lock connect the spacecraft solar panels to the tube for launch.

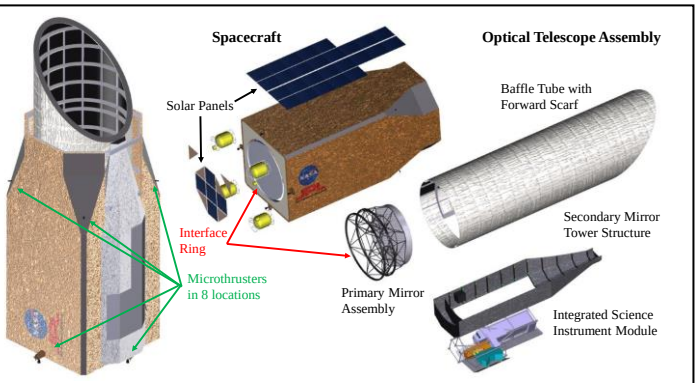

Figure 5: Baseline HabEx Observatory Payload

Figure 6: Payload fits in SLS 8.4m fairing.

The Baseline Observatory is designed for the SLS Block IB mass and volume capacities, and launch environment.[10] The payload fits inside the SLS 8.4-m fairing (Figure 6) with no deployments. The projected total mass (with 30% reserve) of 14-mt (Table 2) has significant margin against the SLS Block-2 capacity of 44 mt to SE-L2. The telescope and spacecraft structure are designed to have a first mode higher than 10 Hz and to survive a 3.5g axial and 1.5g lateral launch load. Table 3 lists the current best mass estimate for each of the telescope's major elements.

Table 2: HabEx Observatory Payload Mass Estimate

Element	CBE [kg]	Reserve [kg]	Total [kg]
Telescope	3431	1029	4460
Science Instruments	1164	499	1663
Spacecraft	4500	1350	5850
Interface Ring	210	63	273
PAF	TBD		
Payload Dry Mass	9305	2941	12246
Propellant	1700		1700
Payload Wet Mass	11005		13946

Table 3: HabEx Optical Telescope Mass Estimate

Component	CBE [kg]
Primary Mirror (with Launch Locks)	1453
Primary Mirror Support	865
Secondary Mirror Assembly	11
Tertiary Mirror Assembly	65
Tower & Baffle Tube	982
Forward Door	55
Total OTA Mass	3431

The baseline structure has a first mode frequency of ~24-Hz. This was accomplished via structurally connecting the secondary mirror tower to the primary stray-light baffle tube (Figure 7). In addition to straylight suppression, the internal baffles provide stiffness. But, because the optical design is off-axis, the baffles rings are not continuous, gussets were added to the tower structure which span the baffle gaps. These gussets eliminated the need for a truss structure – reducing mass and opening the space for instruments. The secondary mirror assembly attaches to the top of the tower and the bottom contains the integrated science instrument module. The tower and tube use TRL-9 composite material M46J with quasi-isotopic laminate properties of 25% 0-deg, 50% 45-deg, 25% 90-deg and a density of 1.58 g/cm^3.

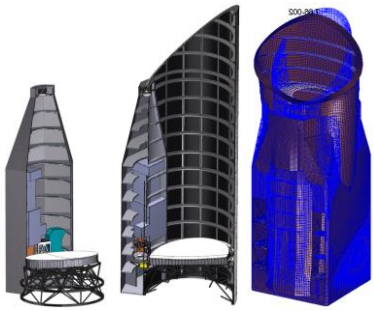

Figure 7: Gussets stiffen Structure

As shown in Figure 5, the telescope is a standalone structure separate from the spacecraft. The spacecraft surrounds the telescope without physically touching it except at the interface ring (which also connects to the launch vehicle payload adapter fixture, PAF). This configuration minimizes the propagation of mechanical disturbances from the spacecraft into the telescope and provides thermal shielding of the telescope while minimizing heat leaks. In fact, STOP modeling predicts that thermal isolation is too good. To increase the primary mirror cold bias, it was necessary to remove portions of the spacecraft anti-sun structure. While the primary and secondary mirrors have active thermal control, the structure does not (although it could be added). The structure is not actively heated because the telescope includes a laser truss system which maintains alignment between the primary, secondary and tertiary mirrors. The laser truss bandwidth is sufficient to sense and correct slow thermal drifts and its noise uncertainty is sufficient to meet the LOS Jitter and LOS WFE stability specifications. Finally, while STOP modeling predicts that the integrated telescope/spacecraft payload's mechanical performance meets the LOS Jitter and LOS WFE stability specification (Section 4), margin can be obtained by adding passive damping (such as Northrop's JWST passive struts) or active vibration isolation (such as Lockheed's disturbance free payload technology) to the interface ring.

3.2 Baseline HabEx Primary Mirror Assembly

Stiffness and mass are important primary mirror design criteria. Stiffness enables performance and simplifies manufacture. The higher a mirror's stiffness, the easier it is to produce the smooth surface needed to achieve 400 nm diffraction limited performance. And, the easier it is to handle (i.e. mount to machinery or simply turning over), which reduces fabrication risk. Also, the higher the mirror's stiffness, the smaller will be its inertial wavefront error and the less likely it is that the mirror will have significant G-release error – both of which are related to gravity sag or self-weight deflection. Mass is important because it provides thermal capacity for a thermally stable mirror. But, the mirror must not be too massive.

The baseline Zerodur® mirror assembly provides an excellent balance between mass and stiffness. The substrate has a flat-back geometry with a 42 cm edge thickness and mass of approximately 1400 kg. (Figure 8) The mirror's free-free first mode frequency is 88 Hz. And, its mounted first mode frequency is 70 Hz. The mirror is locally stiffened to minimize gravity sag.[11] The substrate geometry and mount designs were optimized to produce as uniform as possible XYZ gravity sag deformation. The mirror is attached at three edge locations to a hexapod mount system. This geometry was selected to allow defocus and minimize spherical gravity sag based on vector vortex coronagraph aberration sensitive (Figure 4). Figure 9 shows the baseline mirror's predicted 1-G PV surface gravity sag in global telescope XYZ coordinate system.

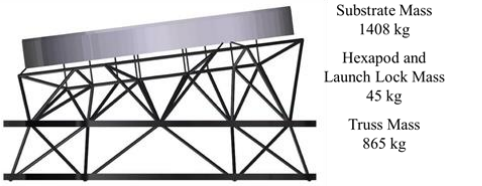

Figure 8: Primary Mirror Assembly

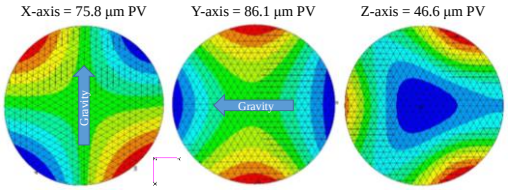

Figure 9: Primary Mirror Gravity Sag (PV surface)

The support structure is a simple truss. It uses TRL-9 M46J with quasi-isotopic laminate properties of 25% 0-deg, 50% 45-deg, 25% 90-deg and a density of 1.58 g/cm3 with a total mass of approximately 865 kg. To minimize WFE stability, the hexapod supports and truss structure are designed for its rigid body and bending modes to be above 40 Hz (Figures 10 and 11).

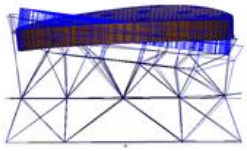
Figure 10: 43.5Hz Rocking Mode

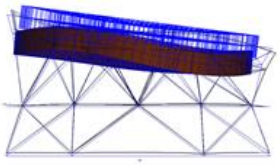
Figure 11: 50Hz Bouncing Mode

Finally, the PM truss structure is designed to accommodate a launch constraint system consisting of 18 axial and 12 radial launch locks (Figure 12). While Zerodur is suitable for applications with mechanical loads from 4.3 to 14.5 psi and when manufactured using Schott's standard surface etch protocol can withstand up to 17.4K psi for short durations[12], standard engineering practice is to limit the maximum launch load to 600 psi. The HabEx launch constraint system is predicted to expose no point on the mirror to greater than 300 psi (Table 4). Without the constraint system, launch stress of as much as 1000 psi is concentrated at the 3 hexapod attachment locations (Figure 13). Finally, if necessary, the launch constraint support structure could also be used as a reaction structure for an active figure control system to mitigate G-release error.

Table 4: Baseline HabEx 4-m Primary Mirror Launch Stress

Acceleration Loads [G]			No-Lock Stress [psi]	Locked Stress [psi]
X	Y	Z		
0.5	0.0	6.0	995	197
0.0	0.5	6.0	959	160
2.0	0.0	3.5	702	297
0.0	2.0	3.5	657	233

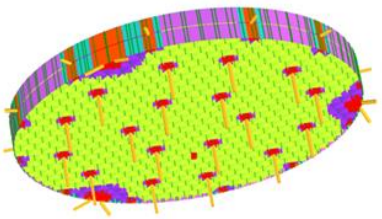
Figure 12: Primary Mirror Launch Constraint systems has 18-axial and 12-radial launch locks

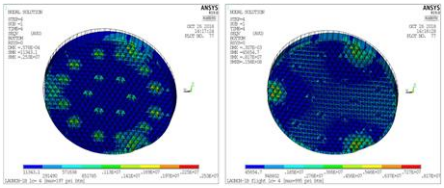

Figure 13: Launch locks redistribute launch stress from the three hexapod attachment locations to the entire mirror.

3.3 Primary Mirror Thermal Control System

The primary mirror thermal control system is critical to the HabEx telescope's ability to achieve science required diffraction limited performance and wavefront stability. The function of the thermal control system is to uniformly set the primary mirror's front surface to the desired operating temperature and keep it at that temperature regardless of where the telescope points on the sky relative to the sun. Control system accuracy impacts diffraction limit performance, signal to noise and spectral throughput. And, the precision to which the system can maintain temperature determines wavefront stability. Any gradient or bias error in the mirror's bulk temperature will introduce a static 'cryo-deformation' wavefront error. And, any temporal variation in the mirror's temperature will introduce instability.

Similar to Hubble, HabEx is cold biasing the primary and secondary mirrors and heating them to the desired operating temperature. The desired operating temperature is constrained by two competing requirements. Near-IR science requires cold mirrors to minimize in-field thermal noise. But, UV science requires that the mirrors to be free of any contamination such as a monolayer of water ice or other out-gassed molecules to maximize spectral throughput. HabEx has selected an operating temperature of 270K for its mirrors because it is above the sublimation temperature for water ice.

The baseline HabEx active radial thermal control concept is an engineering scale-up of systems built by the Harris Corporation. Zonal active thermal control of primary mirrors is currently TRL-9 with systems currently flying on the Harris Corporation commercial 0.7-m and 1.1-m Spaceview™ telescopes. These systems enable on-orbit focus adjustment for optimal image quality.[13,14] Additionally, under the Astrophysics Division funded Predictive Thermal Control Study, Harris Corporation built and delivered to NASA a 1.5-m system with 37 thermal control zones (Figure 14).[15]

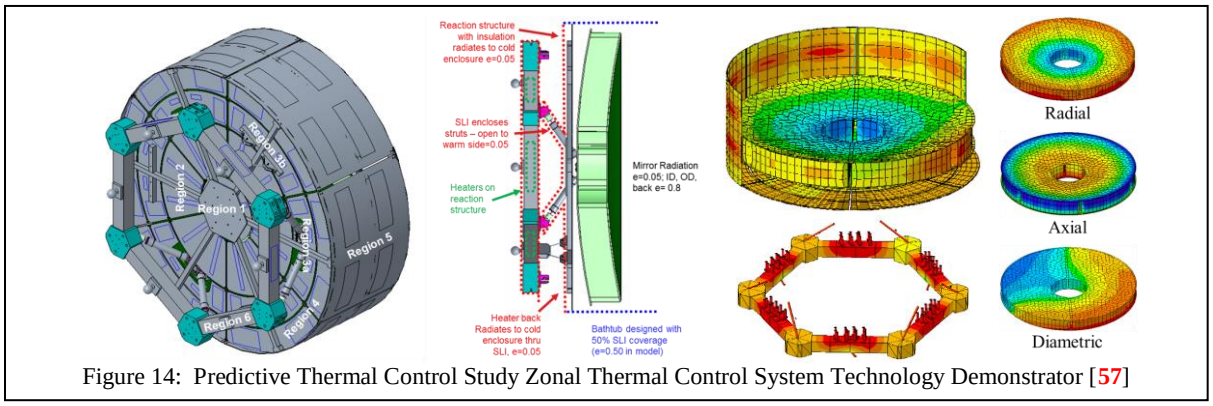

Figure 14: Predictive Thermal Control Study Zonal Thermal Control System Technology Demonstrator [57]

The key to achieving an ultra-stabile thermal wavefront is to sense and correct fluctuations to the mirror's thermal environment faster than the mirror's response time to those changes. The rate at which the primary mirror's RMS surface figure error changes depends on its CTE, mass and thermal capacity.[16] To first order, the larger the mirror's mass and the smaller it's CTE, the smaller and slower its response to a thermal stimuli. These are the reasons why monolithic mirrors fabricated from zero CTE materials such as Zerodur® and ULE® glass are preferred. Current TRL-9 Harris Corp Spaceview™ systems have a noise of ~50-mK and control their 1.1-m telescope to a temperature of 100 to 200-mK.[13,14] STOP analysis shows that the more massive HabEx primary mirror can be controlled to a temperature of ~1-mK with a system having 50-mK noise and 30 second control period.

4. TELESCOPE STRUCTURAL THERMAL OPTO-MECHANICAL PERFORMANCE

4.1 Integrated Model

To evaluate if the baseline HabEx telescope meets its performance requirements, integrated thermal and finite element models (FEM) were constructed of the telescope and spacecraft bus then merged into an observatory model. An observatory level model was required because the telescope's thermal and mechanical performance is strongly influenced by the spacecraft. These models were used to perform structural thermal opto-mechanical performance (STOP) analyses.

4.1.1 Mechanical Model

The FEM was created using the MSC Patran pre-processor and geometry created in Pro-Engineer CAD. The primary and secondary mirror FEMs were created independently using the NASA MSFC developed Arnold Mirror Modeler. Using the integrated NASTRAN model, analyses were performed to ensure strength/stability and stiffness requirements were

satisfied in accordance with NASA-STD5001B and the launch vehicle payload users guide (ULA - Delta IV Heavy). Additionally, the integrated finite element model was used to perform dynamic response, and thermal analysis. Structural elements utilize composite construction where possible to provide a rigid and lightweight design. Where possible, M55J carbon composite material is used due to its excellent strength/stiffness and low mass density (1.58g/cm3) specifications. Telescope structure skins, circumferential ribs, axial webs, and the forward contamination door utilize Honeycomb Sandwich Construction with M55J face sheets with Hexcel honeycomb core. Mirror support truss members assume M55J circular tube construction with titanium end fittings. Full advantage was taken to tailor the M55J unidirectional composite layup orientations for maximum performance and minimum mass. Structural damping is specified to be 0.0005 (.05%).

4.1.2 Thermal Model

The thermal model was created in Thermal Desktop using the geometry created in Pro-Engineer CAD. The Thermal Desktop model has 20K elements and calculates telescope's structure and mirror temperature distribution at 10K nodes. The temperature distribution for each node is mapped onto the NASTRAN FEM and the deflections created by each node's coefficient of expansion (CTE) is calculated using NASTRAN Solution 101. Rigid body motions (RBM) and mirror surface deformations are calculated from the NASTRAN deflections using SigFit.

The thermal control system was designed to maintain the operating temperature of the primary and secondary mirrors at ~270K. Without heaters, the model predicts a primary mirror temperature of 206K and a secondary mirror temperature of 196K. The model assumes TRL-9 capabilities for the enclosure specifications: thermal sensors with 50-mK measurement uncertainty; and proportional controller systems (PID) operating with 30 second periods. The model has a total of 133 control zones. Of these 36 are bang-bang survival heaters set at 212K and 97 are PID control zones (Table 5). The model predicts that the primary mirror front surface will have ~200 mK 'trefoil' gradient. The source of this gradient is thermal conduction into the hexapod struts. And, that the mirror will have ~3 K front to back gradient.

Table 5: Thermal Model Details

Proportional Control Zones	
Primary Mirror Thermal Enclosure	82
Primary Mirror Truss Hexapod Legs	6
Secondary Mirror Thermal Enclosure	9
Bang-Bang Survival Heater Zones	
Telescope Baffle Tube	18
Telescope Secondary Tower	7
Spacecraft Bus Structure	3
Spacecraft Fuel Tanks	8

The primary and secondary mirror coefficient of thermal expansion (CTE) are modeled as consisting of a uniform 'bulk' CTE of 20 ppb/K and a CTE homogeneity distribution of +/- 5 ppb/K (based on test of the Schott 1.2-m mirror).[17] The uniform CTE value determines the mirror's low-order shape response to bulk temperature changes, and/or gradient temperature changes (i.e. axial, radial or lateral). Such temperature changes can produce low-order errors such as power and astigmatism. The homogeneity distribution determines the mirror's mid-spatial response. The model calculates mirror shape changes from two effects: (1) response of mirror with uniform CTE to changes in temperature at each of the 10K nodes; and (2) response of a mirror with a CTE inhomogeneity distribution to a uniform bulk temperature change.

4.1.3 Mechanical Analysis Input

Dynamic mechanical errors (LOS jitter, LOS WFE stability, inertial WFE stability, and impulse ring-down) are caused by structural response to mechanical stimuli. To minimize the source of such stimuli, the baseline HabEx observatory architecture does not use reaction wheels for slewing and pointing. Instead it uses thrusters and micro-thrusters. Thursters slew and point the telescope. They are then turned off and micro-thrusters maintain pointing for the duration of a science exposure. The noise on their thrust is the only source of mechanical stimuli. Micro-thrusters run continuously with variable thrust proportional to applied current, Figure 15 shows a measured noise PSD for a colloidal micro-thruster. The data indicates that micro-thrusters have a maximum noise of about 0.05 μN/√Hz with a roll-off after about 2 Hz.[18] But, because the data is noisy and has not been measured beyond 5 Hz, HabEx is assuming for its dynamic STOP analysis that each micro-thruster head has a flat or 'white' noise spectrum of 0.1 micro-Newton. This specification provides analysis margin. Finally, because the noise 'forcing-function' amplitudes are extremely small, values reported by the analysis could have significant uncertainty. While the FEM's predicted performance is linear as a function of input, the physical system being modeled may not be linear. To mitigate this risk, a model uncertainty factor (MUF) is used in some analysis. In others a MUF is not applied. For each analysis, the MUF status is made explicit.

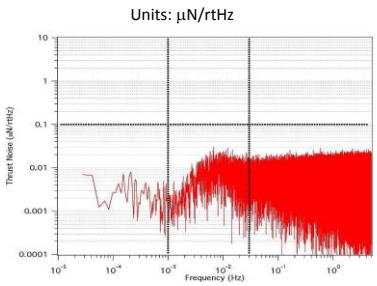

Figure 15: PSD noise plot for colloidal micro-thrusters.[18]

4.1.4 Thermal Analysis Input

Dynamic thermal errors (LOS drift, LOS WFE, and thermal WFE stability) are caused by structural and optical component response to thermal stimuli. To predict thermal performance, design reference missions (DRMs) were analyzed in Thermal Desktop. The calculated temperature distribution is mapped onto the NASTRAN FEM and the deflections of each node calculated. Rigid body motions and surface figure errors (SFE) of the primary and secondary mirrors were calculated from the NASTRAN deflections using SigFit.

The DRM starts by pointing the telescope at a reference star to dig the dark hole. The analysis assumes that the telescope reaches a steady state thermal condition at this sun orientation. Next, the telescope is pointed at the science star. To make the analysis worst-case, it is assumed that this requires a +θ degree pitch away from the sun (Figure 16). To facilitate speckle subtraction, the telescope is rolled +/- Φ degrees about the science star vector (Figure 17).

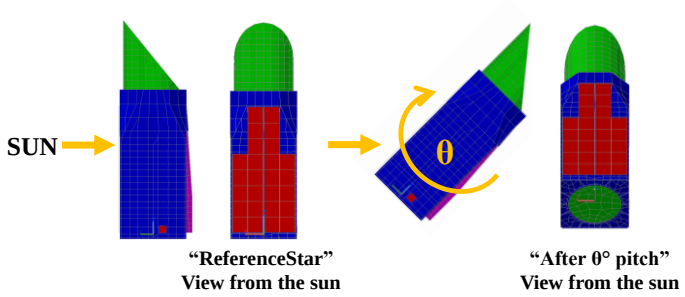

Figure 16: Nominal observing scenario slews for thermal analysis

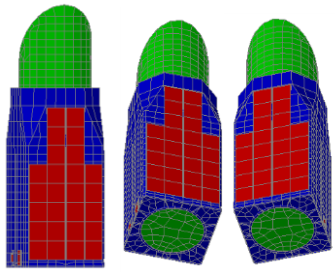

Figure 17: Telescope motions as viewed from the Sun

The specified DRM analyzed is (Figure 18):

- T = 0 hr Drop into SEL2 with observatory pointing 100 degree to Sun
- T = 90 hr Pitch +10 deg away from Sun to Reference Star & 'Dig' Dark Hole
- T = 100 hr Pitch +10 degree to Science Star
- T = 150 hr Roll – 15 degree
- T = 200 hr Roll + 30 degree
- T = 250 hr End Science Observation

The STOP Analysis calculates as a function of DRM (time): Temperature of Primary Mirror (PM) and Secondary Mirror (SM); WFE produced by PM & SM Temp Changes; Relative Rigid Body Motion (RBM) between PM and SM; WFE produced by non-correctable RBM (i.e. after laser truss); and Total Telescope WFE Stability. Figures 19 shows how well the modeled active zonal thermal enclosure controls the temperature of the primary mirror. Once the science observation begins, the primary mirror temperature only changes by +/- 0.15-mK. The primary reason for this stability is the primary mirror's thermal mass. The thermal time constant of the primary mirror is approximately 20 hrs. Please note that roll maneuvers produce negligible thermal error. Also note that, if the science star and reference stars were located such that the sun angle remained unchanged during the slew, i.e. rotate around the sun vector, then there would be no change to the telescope's thermal environment.

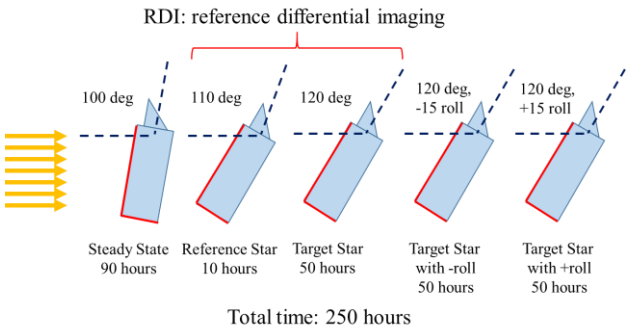

Figure 18: Analyzed Design Reference Mission

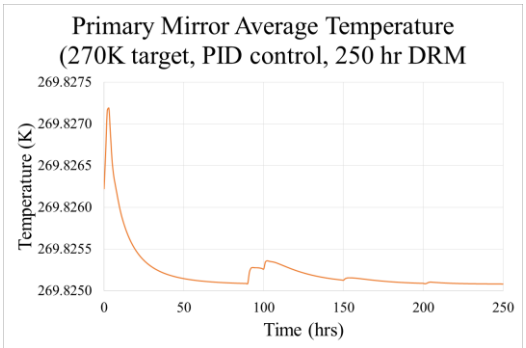

Figure 19: Average PM Temperature for DRM

5. PREDICTED TELESCOPE PERFORMANCE

5.1 Predicted Line of Sight (LOS) Stability Performance

To calculate whether the baseline telescope meets the specification, NASTRAN Multi Point Constraint (MPC) equations created by SigFit were used to determine rigid body displacements of the primary and secondary mirrors relative to the tertiary mirror. Another MPC determined rigid body displacements between the PM and SM. STOP analysis was performed with the integrated FEM and thermal models to calculate the rigid body motions of the primary, secondary and tertiary mirrors caused by mechanical disturbance and thermal drift.

5.1.1 Predicted Mechanical Line of Sight (LOS) Stability Performance

Mechanical LOS stability performance, the rigid-body motion of each mirror was calculated as a result of the structure's response from 0 to 350 Hz to the micro-thruster noise specification applied to the structure from 0 to 10 Hz (Figure 15). The specification provides at least a 2X margin at low frequencies and more margin at higher frequencies. Additionally, a MUF of 4 was applied to amplitudes below 20 HZ, and a MUF of 2 was applied to amplitudes above 20 Hz. Figure 20 shows the predicted displacement of the PM relative to the SM. The red line from 1 to 10 Hz is the initial tolerance defined in Figure 2 to achieve a 0.5 mas LOS stability. And, the red line from 10 Hz to 350 Hz is the maximum displacement for each degree of freedom from the analysis.

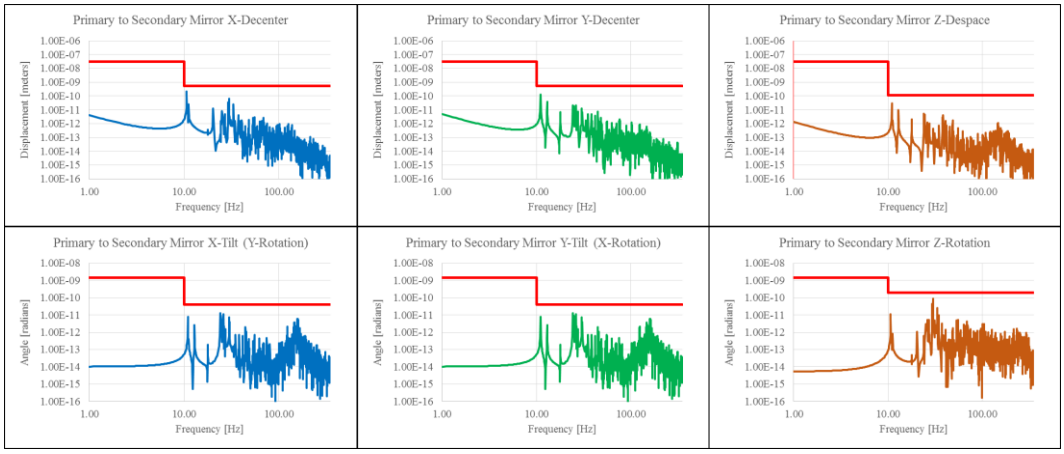

Figure 20: Primary to secondary mirror rigid body amplitudes for micro-thruster noise specification

Figure 20 contains a wealth of information regarding various structural modes and the coupling of those modes with optical components. For example, the displacements that occur between 10 and 12 Hz are associated with a twisting mode between the spacecraft and telescope (Figure 21). The displacements between 25 and 30 Hz are from bending modes of the straylight baffle tube (Figure 7) and bending between the secondary mirror tower and primary mirror truss structure. The displacements in the 45 to 50 Hz range are caused by motions of the primary mirror on its mount (Figures 10 and 11).

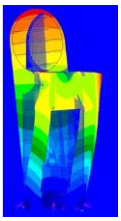

Figure 21: 11-Hz Twist Mode

Table 6 lists the maximum amplitude for each rigid body motion (with MUFs). Collectively, these motions predict an on-sky LOS jitter of less than 0.02 mas (i.e. ~40X performance margin).

Table 6: Predicted maximum rigid body motion of PM and SM from Microthruster Noise

DOF	Δx (nm)	Δy (nm)	Δz (nm)	Θx (nrad)	Θy (nrad)	Θz (nrad)
Primary	0.02	0.02	0.10	0.02	0.02	0.002
Secondary	0.50	0.50	0.01	0.02	0.02	0.20

5.1.2 Predicted Thermal Line of Sight (LOS) Stability Performance

To predict thermal LOS stability performance, the rigid-body motions of each mirror were calculated as a result of the 250-hr DRM discussed in Section 4.1.4. Figures 22 and 23 show the XYZ rigid body residual displacements of the primary and secondary mirrors, i.e. the amount of thermal rigid body motion that is not corrected by the laser metrology system that senses and controls the optical alignment of the primary and secondary mirrors.

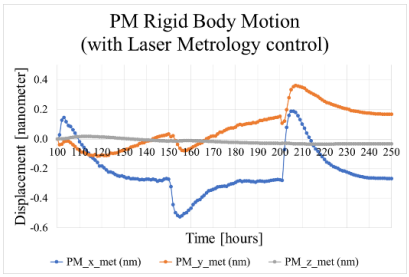

Figure 22: Displacements of PM due to thermal DRM

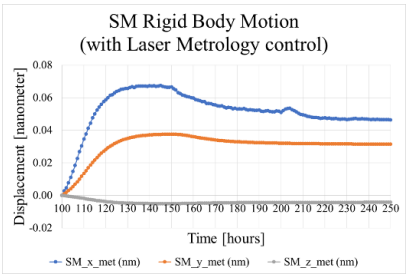

Figure 23: Displacements of SM due to thermal DRM

Table 7 lists the maximum amplitude for each primary and secondary mirror degree of freedom. Collectively, these motions predict an on-sky LOS jitter of approx. 16 mas (i.e. ~3.5X performance margin). In this case, no MUF is applied.

Table 7: Predicted maximum rigid body motion of PM and SM for a Design Reference Mission

DOF	Δx (nm)	Δy (nm)	Δz (nm)	Θx (nrad)	Θy (nrad)	Θz (nrad)
Primary	0.71	0.48	0.05	0.25	0.38	0.39
Secondary	0.07	0.04	0.01	0.01	0.04	0.29

5.1.3 Predicted LOS Stability Performance

RSS'ing the rigid-body motions of the primary, secondary and tertiary mirrors from the STOP mechanical and thermal models (Tables 6 and 7) predicts that the baseline HabEx telescope will have an on-sky line-of-sight stability better than ~13 mas for a 4X margin against the 56 mas specification (Figure 24).

Specification			56.00	mas
			ALLOCATION (one sided PV	
Alignment	Tolerance	units	RSS	Units
PM X-Decenter	0.71	nm	1.22	mas
PM Y-Decenter	0.48	nm	0.80	mas
PM Z-Despace	0.11	nm	0.05	mas
PM Y-Tilt	0.03	n-rad	1.11	mas
PM X-Tilt	0.38	n-rad	12.98	mas
PM Z-Rotation	0.39	n-rad	1.68	mas
SM X-Decenter	0.50	nm	0.77	mas
SM Y-Decenter	0.50	nm	0.74	mas
SM Z-Despace	0.01	nm	0.01	mas
SM Y-Tilt	0.02	n-rad	0.07	mas
SM X-Tilt	0.04	n-rad	0.13	mas
SM Z-Rotation	0.35	n-rad	0.12	mas
TM X-Decenter	0.10	nm	0.02	mas
TM Y-Decenter	0.10	nm	0.02	mas
TM Z-Despace	0.10	nm	0.00	mas
TM Y-Tilt	0.01	n-rad	0.00	mas
TM X-Tilt	0.01	n-rad	0.00	mas
TM Z-Rotation	0.01	n-rad	0.00	mas
RSS LOS Error			13.26	mas

Figure 24: Integrated STOP model predicts ~13 mas on-sky LOS instability (~ 4X margin on specification).

5.2 Predicted Wavefront Error (WFE) Stability

WFE instability can result in dark-hole speckles that produce a false exoplanet measurement or mask a true signal. Sources of WFE instability include LOS, inertial and thermal instability.

5.2.1 Predicted LOS WFE Stability

LOS WFE instability is produced by LOS drift and jitter. Thermal LOS drift and mechanical LOS jitter causes beam-shear on the secondary and tertiary mirrors. And, because these mirrors are conics, beam shear manifests itself as low-order astigmatism and coma. Conic mirrors correct spherical aberration and the shear of full aperture spherical aberration is coma. When viewed over an off-axis sub-aperture, coma appears as astigmatism. Figure 25 shows the predicted WFE instability produced by the LOS predicted in Figure 24 relative to the LOS WFE allocation in the simple VVC-6 error budget of Figure 4. As expected, the largest LOS errors are tilt, power and astigmatism. But these errors are not significant to the VVC-6. The most significant are trefoil and secondary astigmatism. And the predicted amplitudes of these errors have 10X margin relative to their error budget allocation.

					LOS
Index			Allocation LOS		RSS WFE
N	M	Aberration	[pm rms]	MARGIN	(pm rms)
		TOTAL RMS	2528	506	4.998
1	1	Tilt	1351.83	521	2.594
2	0	Power (Defocus)	1010.98	880	1.149
2	2	Astigmatism	1224.08	305	4.013
3	1	Coma	1089.60	1195	0.912
4	0	Spherical	925.42	206106	0.004
3	3	Trefoil	0.51	12	0.043
4	2	Sec Astigmatism	0.28	17	0.017
5	1	Sec Coma	0.25	95	0.003
6	0	Sec Spherical	0.19	12494	0.000
4	4	Tetrafoil	0.49	981	0.000
5	3	Sec Trefoil	0.23	1009	0.000
6	2	Ter Astigmatism	0.14	2405	0.000
7	1	Ter Coma	0.12	18224	0.000
5	5	Pri Pentafoil	0.17	29529	0.000
6	4	Sec Tetrafoil	0.17	58208	0.000
7	3	Ter Trefoil	0.13	132291	0.000
6	6	Hexafoil	0.12	435740	0.000
7	5	Sec Pentafoil	0.12	330417	0.000
7	7	Pri Septafoil	0.14	597064	0.000

Figure 25: LOS WFE stability is predicted to have > 10X margin relative to error budget allocation.

5.2.2 Predicted Inertial WFE Stability

Inertial WFE is similar to the mirror's static (X,Y,Z) gravity sag (i.e. bending of the mirror when it is exposed to a 1G acceleration in the X,Y,Z directions) scaled by the on-orbit acceleration to which it is exposed. Figures 10 and 11 illustrate two such responses: 43.5 Hz rocking and 50 Hz bouncing. Figures 26 and 27 illustrate how the mirror bends as it reacts against the hexapod mount for the rocking and bouncing modes. Please note that inertial WFE is not the same as modal resonant motion.

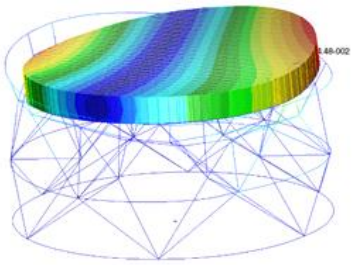

Figure 26: Mirror bending from 49.5 Hz Rocking Mode.

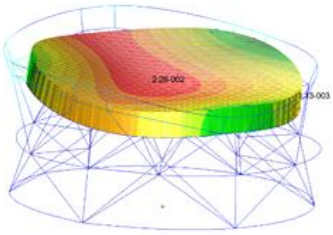

Figure 27: Mirror bending from 50 Hz Bouncing Mode.

To estimate on-orbit acceleration, the observatory FEM was used to calculate XYZ-accelerate from the micro-thrusters at each primary mirror hexapod interface. The absolute maximum XYZ acceleration imparted into the mirror is predicted to be (13-nG, 16-nG, 37-nG). Scaling the RMS gravity-sag WFE of (32.4-µm, 33.2-µm, 21-µm) yields an XYZ RMS inertial WFE of (0.42 pm, 0.53 pm, 0.78 pm). RSSing the components yields a total inertial error of ~1-pm rms.

To check compliance with the error budget inertial tolerance, each gravity sag was decomposed into its Zernike polynomials. These coefficients were scaled by the maximum XYZ acceleration values and RSSed to produce an estimate of the amount of each Zernike wavefront error excited by the micro-thrusters. As expected the term with the smallest margin against the error budget tolerance specification is Trefoil. (Figure 28). Please note that the maximum acceleration values are approximately 10X larger than the average RMS acceleration values. Thus, selecting them for scaling purposes is conservative. Finally, significant additional margin could be obtained by inserting passive or active isolation between the spacecraft and telescope.

			Inertial WFE Stability			Scaled G-Sag Zernikes			Predicted 1 micro-G Gravity Sag		
			Acceleration [µG]		0.042	0.013	0.016	0.037	Zernike Coefficient [pm] RMS Surface		
			Allocation		RSS-Zernikes	X-Zern	Y-Zern	Z-Zern	X-Zern	Y-Zern	Z-Zern
Index			Inertial	MARGIN	[pm rms]	[pm rms]	[pm rms]	[pm rms]	[pm rms]	[pm rms]	[pm rms]
N	M	Aberration	[pm rms]								
		TOTAL RMS	891.94		1.082	0.450	0.570	0.803	34.614	35.613	21.696
1	1	Tilt	1351.83	23951.9	0.056	0.04	0.04	0.02	2.862	2.453	0.436
2	0	Power (Defocus)	1010.98	1711.1	0.591	-0.05	0.00	0.59	-4.220	0.000	15.900
2	2	Astigmatism	1224.08	1683.7	0.727	0.44	0.57	0.11	34.044	35.404	2.937
3	1	Coma	1089.60	48848.1	0.022	0.02	0.01	0.01	1.164	0.481	0.391
4	0	Spherical	925.42	9285.5	0.100	0.01	0.00	-0.10	0.468	0.000	-2.689
3	3	Trefoil	0.51	1.0	0.520	0.01	0.02	0.52	0.757	1.188	14.050
4	2	Sec Astigmatism	0.28	7.9	0.035	0.02	0.02	0.02	1.437	1.305	0.571
5	1	Sec Coma	0.25	192.8	0.001	0.00	0.00	0.00	0.071	0.049	0.013
6	0	Sec Spherical	0.19	23.3	0.008	0.00	0.00	0.01	-0.031	0.000	0.219
4	4	Tetrafoil	0.49	10.3	0.048	0.03	0.03	0.01	2.673	1.999	0.171
5	3	Sec Trefoil	0.23	3.2	0.071	0.00	0.00	0.07	0.093	0.064	1.916
6	2	Ter Astigmatism	0.14	38.5	0.004	0.00	0.00	0.00	0.099	0.042	0.091
7	1	Ter Coma	0.12	451.2	0.000	0.00	0.00	0.00	0.009	0.014	0.002
5	5	Pentafoil	0.17	5.5	0.031	0.02	0.02	0.02	1.296	1.209	0.476
6	4	Sec Tetrafoil	0.17	38.2	0.005	0.00	0.00	0.00	0.164	0.218	0.056
7	3	Ter Trefoil	0.13	27.3	0.005	0.00	0.00	0.00	0.030	0.069	0.124
6	6	Hexafoil	0.12		0.000	0.00	0.00	0.00	0.000	0.000	0.000
7	5	Sec Pentafoil	0.12		0.000	0.00	0.00	0.00	0.000	0.000	0.000
7	7	Septafoil	0.14		0.000	0.00	0.00	0.00	0.000	0.000	0.000

Figure 28: Estimated Inertial Wavefront Error from micro-thruster acceleration.

To predict a more accurate estimate of inertial WFE, NASTRAN calculated the displacement of PM surface nodes from 0 to 350 Hz as a function of the micro-thruster noise specification applied to the structure from 0 to 10 HZ. The WFE produced by these displacements were fit to Zernike polynomials using SigFig. Figure 29 shows the predicted PM inertial WFE for tip/tilt, power, astigmatism, coma, trefoil and spherical. Consistent with the analysis of Figure 55, only trefoil is close to the VVC-6 tolerance specification (red line).

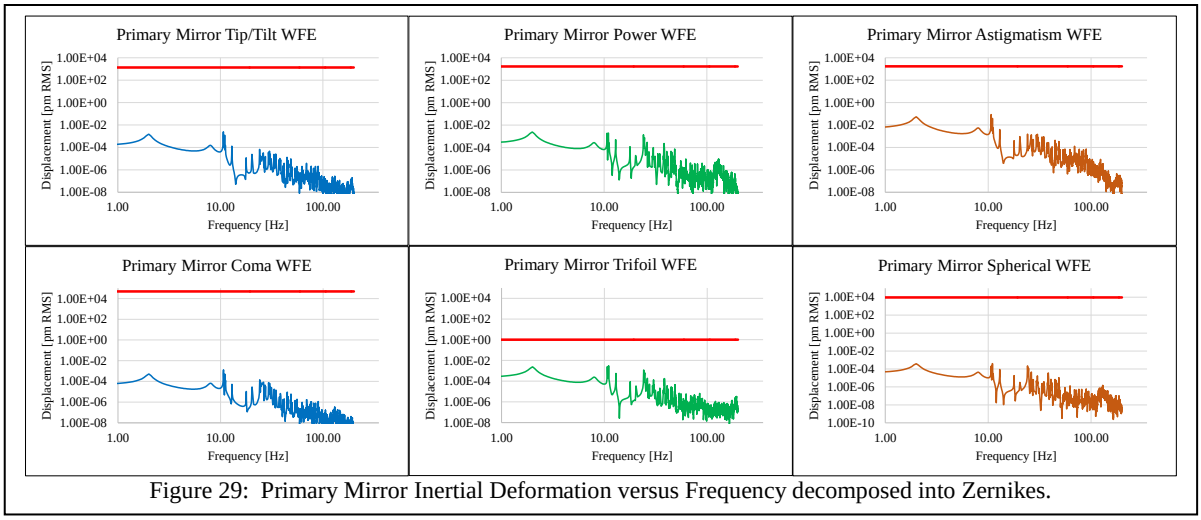

Figure 29: Primary Mirror Inertial Deformation versus Frequency decomposed into Zernikes.

5.2.3 Predicted Thermal WFE Stability

Thermal WFE instability was predicted by applying the DRM discussed in Section 4.1.4 to the integrated model. Thermal Desktop calculated the temperature distribution as a function of time. NASTRAN calculated surface deformations which were then used by SigFit to decompose the temporal WFE into Zernike polynomials as a function of time. Figure 30 shows the predicted change in primary mirror surface figure error decomposed into Zernike polynomials. As symmetric errors, power and trefoil's changes are caused the DRM pitch angle, which changes the total solar load on the telescope. As an asymmetric error, astigmatism's change is caused by the DRM roll which shifts thermal load from one side to the other. Figure 31 shows predicted change for the secondary mirror. Because of its location, it is relatively insensitive to roll.

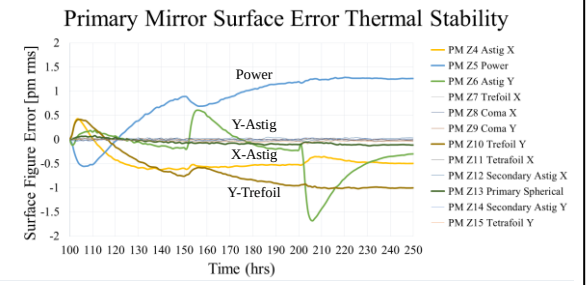

Figure 30: DRM primary mirror SFE changes

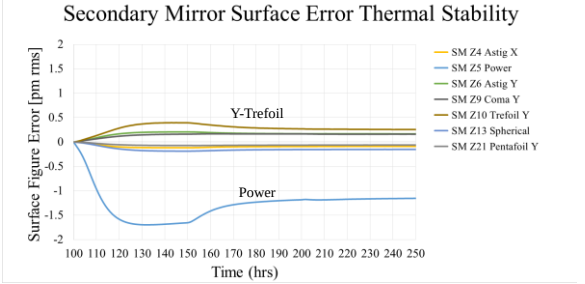

Figure 31: DRM secondary mirror SFE changes

Total predicted DRM wavefront error is was calculated by RSSing the primary and secondary mirror Zernike terms as a function of time. Figure 32 shows the maximum amplitude of each Zernike compared to the simple error budget of Figure 8. Obviously, trefoil is a problem. And margins on the higher order terms are also small. Fortunately there is a solution. Reallocate the error budget.

			Thermal WFE Stability		
			Allocation		Zernike
Index			Thermal	MARGIN	[pm rms]
N	M	Aberration	[pm rms]		
		TOTAL RMS	2528.15		5.565
1	1	Tilt	1351.83	51993.3	0.026
2	0	Power (Defocus)	1010.98	268.9	3.759
2	2	Astigmatism	1224.08	353.5	3.463
3	1	Coma	1089.60	3158.3	0.345
4	0	Spherical	925.42	2285.0	0.405
3	3	Trefoil	0.51	0.2	2.098
4	2	Sec Astigmatism	0.28	2.6	0.108
5	1	Sec Coma	0.25	2.4	0.105
6	0	Sec Spherical	0.19		
4	4	Tetrafoil	0.49	2.6	0.189
5	3	Sec Trefoil	0.23	1.0	0.233
6	2	Ter Astigmatism	0.14		
7	1	Ter Coma	0.12		
5	5	Pentafoil	0.17	0.8	0.217
6	4	Sec Tetrafoil	0.17		
7	3	Ter Trefoil	0.13		
6	6	Hexafoil	0.12		
7	5	Sec Pentafoil	0.12		
7	7	Septafoil	0.14		

Figure 32: Estimated PM/SM Thermal WFE.

5.2.4 Reallocated WFE Stability Error Budget

The error budget defined in Section 2.3 and shown in Figure 8 assumed a simple uniform distribution of contrast leakage. But, because some Zernike terms are more likely to occur than other terms, it is permissible to reallocate contrast leakage from the less likely terms to the more likely terms. Figure 33 shows an optimized error budget for the VVC-6 where the majority of the contrast leakage is allocated to trefoil. The error budget provides a margin of 3.5X for all Zernike terms. This error budget combines the predicted WFE produced by LOS, inertial and

thermal sources. Also, given that STOP analysis shows that trefoil from inertial deformation and thermal DRM is the limiting error, future design iterations might limit its contribution by adding extra vibration isolation to minimize acceleration forces or thermal control at the mount attachment interfaces.

Index			Predicted Performance Amplitude [pm rms]			Total WFE	VVC-6 Sensitivity	Raw Contrast	Allocation	WFE Tolerance	Margin	
N	M	Aberration	LOS	Inertial	Thermal	[pm rms]	[ppt/pm PV]	[ppt]	[ppt]	[pm RMS]		Aberration
		TOTAL RMS	4.998	1.082	5.565	7.558		11.492	40.000	26.306		TOTAL RMS
1	1	Tilt	2.594	0.056	0.026	2.595	0.0002	0.001	0.004	9.030	3.5	Tilt
2	0	Power (Defocus)	1.149	0.591	3.759	3.975	0.0003	0.002	0.008	13.834	3.5	Power (Defocus)
2	2	Astigmatism	4.013	0.727	3.463	5.350	0.0002	0.003	0.009	18.621	3.5	Astigmatism
3	1	Coma	0.912	0.022	0.345	0.975	0.0002	0.001	0.002	3.395	3.5	Coma
4	0	Spherical	0.004	0.100	0.405	0.417	0.0003	0.000	0.001	1.452	3.5	Spherical
3	3	Trefoil	0.043	0.520	2.098	2.162	1.0016	6.125	21.318	7.525	3.5	Trefoil
4	2	Sec Astigmatism	0.017	0.035	0.108	0.115	1.6495	0.599	2.084	0.399	3.5	Sec Astigmatism
5	1	Sec Coma	0.003	0.001	0.105	0.105	1.6645	0.606	2.108	0.366	3.5	Sec Coma
6	0	Sec Spherical	0.000	0.008	0.000	0.008	2.8902	0.062	0.216	0.028	3.5	Sec Spherical
4	4	Tetrafoil	0.000	0.048	0.189	0.195	0.9312	0.574	1.998	0.678	3.5	Tetrafoil
5	3	Sec Trefoil	0.000	0.071	0.233	0.244	1.8200	1.536	5.344	0.848	3.5	Sec Trefoil
6	2	Ter Astigmatism	0.000	0.004	0.000	0.004	2.7219	0.037	0.130	0.013	3.5	Ter Astigmatism
7	1	Ter Coma	0.000	0.000	0.000	0.000	3.0608	0.003	0.011	0.001	3.5	Ter Coma
5	5	Pentafoil	0.000	0.031	0.217	0.219	2.4409	1.854	6.452	0.763	3.5	Pentafoil
6	4	Sec Tetrafoil	0.000	0.005	0.000	0.005	2.2050	0.038	0.131	0.016	3.5	Sec Tetrafoil
7	3	Ter Trefoil	0.000	0.005	0.000	0.005	2.7946	0.053	0.184	0.016	3.5	Ter Trefoil
6	6	Hexafoil	0.000	0.000	0.000	0.000	3.1667	0.000	0.000	0.000	3.5	Hexafoil
7	5	Sec Pentafoil	0.000	0.000	0.000	0.000	3.0694	0.000	0.000	0.000	3.5	Sec Pentafoil
7	7	Septafoil	0.000	0.000	0.000	0.000	2.6510	0.000	0.000	0.000	3.5	Septafoil

Figure 33: Optimized Error Budget for VVC-6.

6. CONCLUSION

The Habitable Exoplanet Observatory Mission (HabEx) is under study for the 2020 Astrophysics Decadal Survey. Its goal is to image and spectroscopically characterize planetary systems in around nearby sun-like stars. Critical to achieving the HabEx science goals is a large, ultra-stable UV/Optical/Near-IR (UVOIR) telescope. The desired telescope is a 4-meter off-axis unobscured three-mirror-anastigmatic, diffraction limited at 400 nm with wavefront stability on the order of a few 10s of picometers. The baseline HabEx telescope is designed using standard engineering practice and its design 'closes'. The telescope's predicted Structural Thermal Optical Performance meets with margin its specified performance error budget allocations for Line of Sight Jitter, LOS Wavefront Error, Inertial WFE and Thermal WFE. Key to meeting its LOS and Inertial specifications is the choice to use micro-thrusters for pointing control instead of reaction wheels. The baseline observatory design fits with margin within the mass and volume constraints of the SLS Block-2 8.4-m fairing.

ACKNOWLEDGEMENTS

This paper is the work of the NASA MSFC HabEx Team and our JPL Collaborators. MSFC Team: Michael Effinger, Scott Smith, Thomas Brooks, Jacqueline Davis, Brent Knight, Mark Stahl; Willian Arnold (AI Solution); Mike Baysinger, Jay Garcia, Ron Hunt, Andrew Singleton, Mary Caldwell and Melissa Therrell (ESSA); Bijan Nemati (UAH); and interns Jonathan Gaskin (UNCC), Jonathan McCready (NCSU), and Hao Tang (UoMI). JPL Team: Keith Warfield, Gary Kuan, Stefan Martin, Velibor Cormarkovic, Scott Howe, Juan Villalvazo, Stuart Shaklan, and Team X.

REFERENCES

[1] Committee for a Decadal Survey of Astronomy and Astrophysics; National Research Council, New Worlds, New Horizons in Astronomy and Astrophysics, The National Academies Press, Washington, D.C., 2010.

[2] Stahl, H. Philip, "Overview of a telescope concept design for the Habitable-zone Exoplanet Direct Imaging Mission", Proc. SPIE 10398, UV/Optical/IR Space Telescopes and Instruments: Innovative Technologies and Concepts VIII, 1039806 (5 September 2017); doi: 10.1117/12.2275192; http://dx.doi.org/10.1117/12.2275192

[3] Stahl, H. Philip, "Overview and performance prediction of the baseline 4-meter telescope concept design for the habitable-zone exoplanet observatory", Proc. SPIE 10698, Space Telescopes and Instrumentation 2018: Optical, Infrared, and Millimeter Wave, 106980W (6 July 2018); doi: 10.1117/12.2315291; https://doi.org/10.1117/12.2315291

[4] Harvey, James E. and Christ Ftaclas, "Diffraction effects of telescopes secondary mirror spiders on various image-quality criteria", Applied Optics, Vol. 34, No. 28, pp-6337, 1 Oct 1995.

[5] Nemati, Bijan, H. Philip Stahl, Mark T. Stahl, and Garreth Ruane "HabEx Telescope WFE stability specification derived from coronagraph starlight leakage", Proc. SPIE 10743, Optical Modeling and Performance Predictions X, 107430G (17 September 2018); doi: 10.1117/12.2312662;
[6] Morgan, Rhonda H., et. al., "HabEx yield modeling with for systems engineering", SPIE 10398-3, 2017.
[7] NASA, Exo-C: Imaging Nearby Worlds, CL#15-1197, March 2015 https://exep.jpl.nasa.gov/stdt/Exo-C_Final_Report_for_Unlimited_Release_150323.pdf
[8] Stuart Shaklan, private communication, 10 Aug 2017
[9] Garrett Ruane, private communication, June 2017
[10] Stahl, H. Philip, Randall C. Hopkins, Andrew Schnell, David Alan Smith, Angela Jackman, Keith R. Warfield, "Designing astrophysics missions for NASA's Space Launch System," J. Astron. Telesc. Instrum. Syst. 2(4), 041213 (2016), doi: 10.1117/1.JATIS.2.4.041213
[11] Arnold, William R., H. Philip Stahl, "Design trade Study for a 4-meter off-axis primary mirror substrate and mount for the Habitable-zone Exoplanet Direct Imaging Mission", Proc. SPIE 10398, UV/Optical/IR Space Telescopes and Instruments: Innovative Technologies and Concepts VIII, 1039808 (5 September 2017); doi: 10.1117/12.2275193;
[12] Peter Hartmann, "Minimum lifetime of ZERODUR® structures based on the breakage stress threshold model: a review," Optical Engineering, 58(2), 020902 (2019), doi: 10.1117/1.OE/58.2.020902
[13] Harris Corporation, "SpaceviewTM 50/65/70 Small Satellite Imaging Soluitions" Specification Data Sheet, harris.com, 2019.
[14] Harris Corporation, "SpaceviewTM 110 Satellite Imaging Solution" Specification Data Sheet, harris.com, 2019.
[15] Harris Corporation, "PTC Thermal System Design Review", NASA Marshall Space Flight Center Contract NNM15AA01C, AMTD II, 17 July 2018,
[16] Brooks, Thomas, H. P. Stahl, William R. Arnold, "Advanced Mirror Technology Development (AMTD) thermal trade studies", Proc. SPIE. 9577, (September 23, 2015) doi: 10.1117/12.2188371
[17] Brooks, Thomas E., Ron Eng, Tony Hull, H. Philip Stahl, "Modeling the Extremely Lightweight Zerodur Mirror (ELZM) thermal soak test", Proc. SPIE 10374, Optical Modeling and Performance Predictions IX, 103740E (6 September 2017); doi: 10.1117/12.2274084
[18] Ziemer, et. al., "Colloid Micro-Newton Thrusters for Precision Attitude Control", CL#17-2067, April 2017.